MicroRNAs contribute to the host response to *Coxiella burnetii*

Madhur Sachan[1,2], Katelynn R. Brann[3], Daniel E. Voth[3], Rahul Raghavan[1,4]*

[1]Department of Biology, Portland State University, Portland, OR, 97201, USA.

[2]Department of Medicine, Cardiovascular Division, Brigham and Women's Hospital, Harvard Medical School, Boston, MA, USA 02115.

[3]Department of Microbiology and Immunology, University of Arkansas for Medical Sciences, Little Rock, AR, 72205, USA.

[4]Department of Molecular Microbiology and Immunology, The University of Texas at San Antonio, San Antonio, TX, 78249, USA.

*Author for correspondence:

Rahul Raghavan | Email: rahul.raghavan@utsa.edu

Key words: *Coxiella burnetii*, miRNA, macrophage, apoptosis, autophagy, infection

ABSTRACT

MicroRNAs (miRNAs), a class of small non-coding RNAs, are critical to gene regulation in eukaryotes. They are involved in modulating a variety of physiological processes, including the host response to intracellular infections. Little is known about miRNA functions during infection by *Coxiella burnetii*, the causative agent of human Q fever. This bacterial pathogen establishes a large replicative vacuole within macrophages by manipulating host processes such as apoptosis and autophagy. We investigated miRNA expression in *C. burnetii*-infected macrophages and identified several miRNAs that were down- or up-regulated during infection. We further explored the functions of miR-143-3p, an miRNA whose expression is down-regulated in macrophages infected with *C. burnetii*, and show that increasing the abundance of this miRNA in human cells results in increased apoptosis and reduced autophagy – conditions that are unfavorable to *C. burnetii* intracellular growth. In sum, this study demonstrates that *C. burnetii* infection elicits a robust miRNA-based host response, and because miR-143-3p promotes apoptosis and inhibits autophagy, down-regulation of miR-143-3p expression during *C. burnetii* infection likely benefits the pathogen.

INTRODUCTION

The highly infectious intracellular pathogen *Coxiella burnetii* is the etiological agent of Q fever (1–3). After uptake by a host cell, typically an alveolar macrophage, *C. burnetii* establishes a replicative niche termed the *Coxiella*-containing vacuole (CCV) that matures by fusing with lysosomal, autophagic, and secretory vesicles (4–6). To facilitate intracellular replication, *C. burnetii* secretes effector proteins into the host cytosol using a Dot/Icm Type IVB secretion system (T4SS) that disrupt several host processes, including apoptosis, lipid metabolism, inflammation, and vesicular trafficking (3, 7–12). For instance, *C. burnetii* inhibits host apoptosis by recruiting anti-apoptotic Bcl-2 to the CCV, inactivating pro-apoptotic Bad, and promoting a pro-survival response by activating Erk1/2, Akt, and PKA signaling (13–16). Similarly, autophagy-related proteins such as LC3 and p62 are recruited to CCV in a T4SS-dependent manner (10, 17), and inhibition of autophagy components results in reduced *C. burnetii* replication (18, 19).

MicroRNAs (miRNAs) are a class of single-stranded, small (~22 nucleotides), non-coding RNAs that orchestrate post-transcriptional gene regulation in eukaryotes and some viruses (20). In humans, miRNAs regulate a large number of genes, primarily by inhibiting target gene expression via translation repression and messenger RNA (mRNA) degradation (21–23). Studies have shown that miRNAs are integral to the host response to bacterial, viral, and parasitic infections (24–31); however, miRNAs could either promote or inhibit infection. For example, induction of miR-142-3p expression in macrophages leads to down-regulation of N-Wasp, an actin-binding protein, resulting in reduced uptake of *Mycobacterium tuberculosis* (32). Conversely, induction of miR-125a-3p in macrophages inhibits autophagy and phagosomal

maturation, which favors intracellular survival of *M. tuberculosis* by promoting autophagosomal escape (33).

Expression of miRNAs is perturbed in macrophages infected with *C. burnetii* (34), but their potential roles are unknown. In this study, we investigated macrophage gene expression across five time-points during *C. burnetii* infection and identified a large number of miRNAs and protein-coding genes that were differentially expressed, suggesting their involvement in the host response to infection. We also demonstrate that transfecting host cells with miR-143-3p results in reduced *C. burnetii* growth, enhanced apoptosis and diminished autophagy. Collectively, our data indicate that an intracellular environment with a low level of miR-143-3p is conducive to *C. burnetii* growth.

RESULTS

Host gene expression correlates with bacterial growth

To identify infection-associated miRNAs and their potential mRNA targets, we measured miRNA and protein-coding gene expression in THP-1 macrophages infected with *C. burnetii* Nine Mile RSA439 Phase II (NMII). The total number of differentially expressed (log2 fold-change ≥ 0.75, Padj ≤ 0.05) miRNAs and mRNAs increased from 25 to 60 and 454 to 6,525, respectively, from day 1 to day 3 (**Table 1 and S1**). By day 5, far fewer miRNAs and protein-coding genes ((34, 211, respectively) were up- or down-regulated in *C. burnetii*-infected cells. This pattern of gene expression suggests that the magnitude of the host cell response to *C. burnetii* infection increases as the bacterium actively replicates (day 3), and as LCVs transition to metabolically less active SCVs (day 5) (35), host response becomes muted in tandem.

miRNAs potentially regulate multiple host signaling pathways during *C. burnetii* infection

To identify genes and metabolic pathways targeted by miRNAs, we first performed inverse-expression pairing using the Ingenuity Pathway Analysis (IPA) tool (36). We selected miRNAs and their known or predicted target genes that showed an inverse pattern of expression in *C. burnetii*-infected cells. For instance, if expression of an miRNA is up-regulated in *C. burnetii*-infected cells, we chose targets that are down-regulated, and vice versa. This analysis identified 14, 18, 25, 51, and 23 miRNAs at 8 h, 24 h, 48 h, 72 h, and 120 h post-infection (hpi), respectively, that were inversely paired with differentially-expressed target mRNAs **(Table S2)**. We then investigated biochemical pathways that were enriched for these proteins using the Core Analysis function in IPA, which revealed 215 pathways, including apoptosis signaling, PI3K/AKT, and autophagy that are likely regulated by miRNAs **(Figure 1, Table S3)**. To investigate the role of miRNAs in apoptosis, a process known to be important during *C. burnetii* infection (13, 37–40), we measured expression of 84 miRNAs associated with apoptosis using a targeted qPCR array (41). This assay showed that 12 miRNAs were up- or down-regulated in *C. burnetii*-infected cells at 72 hpi (**Table 2**), suggesting their involvement in apoptosis regulation as part of the host response to *C. burnetii*.

miR-143-3p is down-regulated in *C. burnetii*-infected human alveolar macrophages

Among apoptosis-related miRNAs, we focused on miR-143-3p, which was significantly down-regulated in NMII-infected THP-1 cells (**Table 2, Figure 2A**). Because NMII is an avirulent laboratory strain and THP-1 cells are not natural host cells for *C. burnetii*, we measured miR-143-3p expression using primary human alveolar macrophages (hAMs) infected with the fully virulent *C. burnetii* Nine Mile RSA493 Phase I (NMI) strain. At 72 hpi, expression of miR-143-

3p was significantly down-regulated in hAMs infected with *C. burnetii* (**Figure 2B**). Intriguingly, expression of miR-143-3p was significantly lower in NMI-infected than in NMII-infected hAMs. While the cause for this disparity is currently unknown, the full-length lipopolysaccharide (LPS) present in NMI might play a role because LPS is known to repress transcription of the miR-143/145 gene cluster (42).

Increased miR-143-3p expression inhibits *C. burnetii* growth

Because expression of miR-143-3p is down-regulated during *C. burnetii* infection, we tested how higher levels of miR-143-3p in host cells would impact intracellular growth. We first transfected HeLa cells with either miR-143-3p or a non-specific control miRNA (miR-control) and then infected cells with NMII and measured bacterial growth at 48 hpi. As shown in **Figure 3**, *C. burnetii* grew significantly better in untransfected and miR-control-transfected cells compared to miR-143-3p-transfected cells, indicating that an intracellular environment with low levels of miR-143-3p could be advantageous to the pathogen.

Early apoptosis is enhanced in cells transfected with miR-143-3p

To test the impact of miR-143-3p on apoptosis, we transfected HeLa cells with either miR-143-3p or miR-control and assessed early- and late-stage apoptosis using annexin V-PE and eFluor780 staining followed by flow cytometry (43). We observed that the percentage of early, but not late, apoptotic cells in the miR-143-3p-transfected population was significantly higher than in cells transfected with miR-control (**Figure 4**). To begin to understand miR-143-3p's regulatory circuit, we assessed expression of *akt1* (AKT Serine/Threonine Kinase 1) and *bcl2* (B-cell lymphoma 2), two genes targeted by miR-143-3p that are central to apoptosis regulation in

human macrophages (**Figure S1**) (44–47). Expression *of akt1* and *bcl2* genes and levels of activated Akt and Bcl-2 proteins were significantly reduced in miR-143-3p-expressing cells compared to cells transfected with miR-control (**Figure 5)**. Together, our data suggest that lower levels of miR-143-3p present in *C. burnetii*-infected cells increases expression of *akt1* and *bcl2*, which likely stalls apoptosis induction, thereby supporting the pathogen's intracellular growth.

miR-143-3p has potential roles in autophagy

Analysis of miRNA-targeted pathways indicated that miRNAs could also be involved in autophagy **(Table S3)**, a process that is interconnected with apoptosis and is involved in the host response to *C. burnetii* (18, 48–50). We measured rapamycin-induced autophagic flux in HeLa cells transfected with either miR-143-3p or miR-control and observed that autophagic flux was slightly, but significantly, lower in miR-143-3p-transfected cells compared to miR-control-transfected cells (**Figure 6**). Several genes involved in autophagy, including *atp6v1a* (V-type proton ATPase catalytic subunit A) and *slc7a11* (Solute Carrier Family 7 Member 11) are controlled by miR-143-3p (24, 25). We observed significantly reduced expression of *atp6v1a* and *slc7a11* and concordant reduction in their encoded proteins (VATA and xCT, respectively) in miR-143-3p-transfected cells compared to control cells **(Figure 7, Table S4)**, indicating a role for these genes in reduced autophagic flux in miR-143-3p-expressing cells.

DISCUSSION

In this study, we show, for the first time, that *C. burnetii* infection elicits a robust miRNA-based host response, and closer examination of miR-143-3p function revealed that the miRNA promotes apoptosis and inhibits autophagy. This combination of phenotypes potentially produces

an intracellular environment that is not conducive *to C. burnetii* growth, likely explaining down-regulation of miR-143-3p expression during *C. burnetii* infection. miR-143-3p presumably antagonizes *C. burnetii* growth by modulating components of the PI3K-Akt signaling network, which controls diverse host cell functions (**Figure S1**) (51). Activation of Akt by P13K induces expression of pro-survival Bcl-2 and inhibits pro-apoptotic proteins such as Bad (52), leading to decreased caspase-3 activation and subsequent inhibition of intrinsic apoptosis. During *C. burnetii* infection, Akt is activated, Bcl-2 is recruited to CCVs, and the pathogen secretes effector proteins that inhibit apoptosis (15, 16, 39, 53). Our results add to this knowledge by demonstrating that levels of Akt and Bcl-2 are significantly reduced and early apoptosis is significantly enhanced in cells transfected with miR-143-3p. No significant difference is evident in late apoptosis, a process characterized by DNA fragmentation, suggesting that miR-143-3p does not affect this process.

In addition to inhibiting apoptosis, *C. burnetii* manipulates autophagy to generate CCVs (10, 18, 49, 50). Interestingly, miR-143-3p appears to inhibit autophagy, and several genes involved in this process, including *atp6v1a* and *slc7a11*, are regulated by miR-143-3p (23–25, 54–57). Expression of both genes is significantly reduced in miR-143-3p-transfected cells, indicating that the miRNA's effect on autophagy involves regulation of v-ATPase and cystine/glutamate antiporter xCT. In accordance with our results, inhibition of autophagy causes improper CCV maturation and reduces intracellular *C. burnetii* growth (17, 58, 59). Inhibition of ATP6V1A, a catalytic subunit of the lysosomal v-ATPase, likely disrupts autophagic flux by inhibiting V-ATPase-dependent acidification of developing CCV, thereby reducing *C. burnetii* growth (56). Furthermore, inhibition of xCT (encoded by *slc7a11*), a cystine/glutamate antiporter that relies on autophagy machinery to import cystine, could deprive the pathogen of cysteine, an

amino acid essential to its growth (55, 60, 61). Finally, although this needs to be confirmed in macrophages, overexpression of miR-143-3p in human endothelial progenitor cells decreased LC3-II and increased p62 levels, two phenotypes that strongly imply a role for miR-143-3p in dampening autophagic flux (62). Cumulatively, our data suggest that down-regulation of miR-143-3p during *C. burnetii* infection promotes intracellular growth of the pathogen by delaying apoptosis and promoting autophagy. Further studies are required to determine if this is a *C. burnetii*-driven process and if LPS and/or T4SS effectors promote pathogen growth by down-regulating miR-143-3p expression.

MATERIALS AND METHODS

Bacterial strains and growth conditions

Coxiella burnetii Nine Mile RSA439 (Phase II, Clone 4) isolate (NMII) was cultured in acidified citrate cysteine medium-2 (ACCM-2) for 7 days at 37°C, 5% CO_2, 2.5% O_2 (63). Bacteria were quantified using PicoGreen (64, 65), collected by centrifugation (3000 x g,10 min, 4°c), resuspended in PBS containing 0.25 M sucrose (PBSS), and stored at -80°C until further use. Before infection, THP-1 cells (American Type Culture Collection, TIB-202) were differentiated into adherent, macrophage-like cells in RPMI-1640 supplemented with 1 mM sodium pyruvate, 0.05 mM beta-mercaptoethanol, 4500 mg/L glucose, and 10% heat-inactivated fetal bovine serum (FBS) at 37°C under 5% CO2 for 24 h using 30 nM phorbol 12-myristate 13-acetate (PMA), followed by 24 h of rest in PMA-free medium. Cells were infected with NMII at a multiplicity of infection (MOI) of 25 in serum-free growth medium for two hours and this time-point was considered to be 0 hpi. To remove extracellular bacteria, cells were washed three times with PBS followed by replacement with complete growth medium, which was replaced

198 with fresh medium at 72 hpi. Primary human alveolar macrophages (hAMs) were harvested by
199 bronchoalveolar lavage (BAL) from postmortem human lung donors and infected with either
200 NMI (*C. burnetii* Nine Mile Phase I RSA493) or NMII at 25 MOI. hAMs were cultured at 37°C
201 under 5% CO_2 in Dulbecco's modified Eagle/F-12 (DMEM/F12) medium (Gibco) containing
202 10% FBS for 72 hpi, as described previously (66).
203
204 **Transfection of HeLa cells**
205 miRCURY LNA hsa-miR-143-3p and miRNA negative control were purchased from Qiagen.
206 The negative control (miR-control) is a non-specific miRNA that shows no homology to any
207 known miRNA or mRNA sequences annotated in mouse, rat, or human genomes. HeLa cells
208 were reverse transfected with miRNAs as previously described (67). Briefly, 25 nM (final
209 concentration) of either miR-143-3p mimic or miR-control was incubated in HiPerFect
210 Transfection Reagent (Qiagen) for 10 min at room temperature to allow formation of transfection
211 complexes. Transfection complexes were uniformly spotted at the bottom of each well of a 24-
212 well tissue culture plate and 3.5×10^4 HeLa cells were added to each well and incubated in
213 OptiMEM medium. After 24 h, the medium was removed, and cells were washed twice with
214 PBS before infection with NMII at an MOI of 100 in serum-free DMEM medium for two hours
215 followed by washing and replenishing cells with serum-containing DMEM medium for
216 experiments at 48 hpi.
217
218 **Intracellular growth assay**
219 *C. burnetii* growth was measured at 48 hpi in HeLa cells transfected 24 h prior to infection with
220 either miR-143-3p or miR-control. To quantify intracellular bacteria using qPCR, total DNA was

extracted using QIAamp DNA Mini Kit (Qiagen) according to the manufacturer's instructions and SYBR Green-based qPCR was performed using *C. burnetii*-specific primers (**Table S5**), as described previously (65). Quantification cycle (Cq) values were converted to bacterial genome equivalents (GE) using a standard curve, as described previously (64). Since qPCR-based quantitation does not differentiate between live and dead cells, we independently quantified viable intracellular bacteria by enumerating colony forming units (CFUs), as described previously (68, 69). Briefly, infected host cells were lysed in ice-cold water for 40 min at 4°C followed by repeated pipetting with a syringe and 25G needle to lyse remaining cells, centrifuged for 10 min at 70 x g (4°C) followed by centrifugation of supernatants for 1 min at 13,500 x g (4°C). Pellets were resuspended in ACCM-2, serially diluted, and spot-plated on ACCM-2 containing 0.5 mM tryptophan and 0.5% agarose. Plates were incubated for 10 days at 37°C, 5% CO_2, and 2.5% O_2 before enumerating CFUs.

RNA sequencing, miRNA-target interactions and pathway analysis

THP-1 macrophages infected with NMII (MOI of 25) and uninfected controls were analyzed at 8, 24, 48, 72, and 120 hpi for miRNA and mRNA expression. At each time point, growth medium was replaced with 1 ml of TRI reagent (Life Technologies) and total RNA was extracted and treated with DNase (Invitrogen) per the manufacturer's instructions. Samples were sequenced using Illumina NovaSeq 6000 for mRNAs and Illumina HiSeq 2500 for miRNAs at the Yale Center for Genome Analysis or Novogene Corporation, Sacramento, CA. Sequencing reads were mapped to the reference human miRNA (miRbase 22.1) or genome (GRCh38) databases using CLC Genomics Workbench v6.5 (Qiagen) (70, 71). Differential gene expression (log2 fold-change ≥ 0.75; adjusted p-value ≤ 0.05, Wald test) between NMII-infected and

uninfected cells was calculated using DESeq2 (72). Inverse-expression pairings of differentially-expressed miRNAs and mRNAs and IPA core analysis of differentially-expressed genes were performed using Ingenuity Pathway Analysis (IPA, Qiagen) (36).

Quantitative Reverse Transcription PCR (qRT-PCR)

Expression of 84 apoptosis-related miRNAs was measured using a miScript miRNA PCR Array Human Apoptosis kit (Qiagen). Briefly, total RNA extracted from infected or uninfected macrophages at 72 h pi (n = 3) were reverse transcribed using a miScript II RT kit and HiSpec buffer (Qiagen) and qPCR reactions were performed on a Stratagene Mx3005P Real-Time PCR system. miRNA expression data were normalized using the global quantitation cycle (Cq) mean of expressed miRNAs, and relative miRNA expression levels were calculated using the delta-delta Cq method (73). Expression of *akt1*, *bcl2*, *atp6v1a*, and *slc7a11* was quantified using qRT-PCR using *gapdh* primers as an endogenous reference control, as described previously (65). Briefly, total RNA was extracted, DNase-treated, and cDNA generated using RevertAid First Strand cDNA Synthesis Kit (Thermo Scientific). To perform qPCR, cDNA templates were diluted and mixed with gene-specific primers and SYBR Green (Applied Biosystems) in a 20 µl reaction according to the recommended protocol (Applied Biosystems). Primers used in this study are listed in **Table S5**. To assay miR-143-3p expression in hAMs, PCR primers for miR-143-3p and the endogenous reference *rnu*6 (small nuclear ribonucleic acid) were procured from Qiagen and qRT-PCR reactions were performed as described above.

Apoptosis assay

Apoptosis was quantified in HeLa cells transfected with miR-143-3p or miR-control using Annexin V-PE (Invitrogen) and Fixable Viability Dye eFluor780™ (Invitrogen) (43). At 72 h post-transfection, cells were treated with trypsin, stained with efluor780 Fixable Viability Dye for 30 min in dark (4°C), followed by staining with Annexin V-PE for 15 min per the recommended protocol (Invitrogen). Cells were immediately assayed for early apoptosis (Annexin V-PE positive and eFluor780 negative) and late apoptosis/necrosis (Annexin V-PE positive and eFluor780 positive) markers using a FACSAria Fusion flow cytometer (BD Biosciences). Fluorescence parameters were gated using unstained and single-stained cells and a total of 10,000 events were counted for each sample using FACSDiva Software (BD Biosciences).

Autophagic flux assay

CYTO-ID Autophagy Detection Kit 2.0 (ENZ-KIT175, Enzo Life Sciences) was used to quantify autophagic flux at 72 h post transfection on HeLa cells transfected with either miR-143-3p or miR-control. Cells were treated with media containing 200 nM rapamycin for 16 h to induce detectable levels of autophagy (74, 75), washed, and incubated for 30 min at 37°C in Microscopy Dual Detection Reagent containing CYTO-ID green detection reagent and Hoechst 33342 nuclear stain in 1X assay buffer. Three sets of at least 200 cells per well were immediately analyzed using a fluorescence microscope (Keyence Corporation) and levels of autophagic flux were measured as average CYTO-ID green brightness per cell calculated using Keyence BZ-X700 software (76, 77).

Multiplex immunoassay

Activation (phosphorylation) of proteins involved in early apoptosis, including Akt (pS473) and Bcl-2 (Ser70), were quantified using 7-Plex Early Apoptosis Magnetic Bead Kit (EMD Millipore). Total cell lysate from HeLa cells transfected with miR-143-3p or miR-control was prepared using Lysis Buffer containing protease inhibitors, followed by bicinchoninic acid (BCA) quantitation at 72 h post-transfection. Briefly, 17.5 µg/well of diluted cell lysate was added to 1X magnetic beads at 1:1 ratio in a 96-well plate. The plate was incubated on a plate shaker (4°C, 700 rpm, dark) for 18 h, followed by washing and incubation with 1X Detection Antibody for 60 min at room temperature (RT) with shaking (700 rpm, dark). The detection antibody was then removed, and samples were incubated for 15 min at RT in the dark with 1X Streptavidin-PE (SAPE) followed by 15 min incubation (RT, dark) with the amplification buffer. SAPE and amplification buffer were removed, and beads were resuspended in 150 µl of assay buffer to analyze median fluorescence intensity (MFI) using a Luminex 200 system.

Quantitative mass spectrometry

Total cell lysate from HeLa cells transfected with either miR-143-3p or miR-control were collected at 48h post-transfection in triplicates. TMT labeling and mass spectrometry were performed at the Proteomics Shared Resource facility at Oregon Health & Science University, as described previously (78). Briefly, samples were lysed, sonicated, and heated at 90°C for 10 min followed by overnight micro-digestion of each sample using an S-trap micro protocol. Peptides were labelled with TMT6-plex reagents, and multiplexed TMT-labeled samples were separated by two-dimensional reversed-phase-reversed-phase (2DRPRP) liquid chromatography on a Orbitrap Fusion Tribrid instrument (Thermo Scientific). Proteins were identified by searching

against the human proteome in UniProt, and TMT reporter ion intensities were processed with in-house scripts. Differential protein abundance was determined by the Bioconductor package edgeR.

Data availability

Sequencing reads from this study have been deposited on NCBI Sequence Read Archive (SRA) under the BioProject accession PRJNA679931.

ACKNOWLEDGEMENTS

This work was supported in part by National Institutes of Health grants AI123464 and AI133023 to R.R.

REFERENCES

1. Gürtler L, Bauerfeind U, Blümel J, Burger R, Drosten C, Gröner A, Heiden M, Hildebrandt M, Jansen B, Offergeld R, Pauli G, Seitz R, Schlenkrich U, Schottstedt V, Strobel J, Willkommen H. 2014. *Coxiella burnetii* - Pathogenic Agent of Q (Query) Fever. Transfus Med Hemother 41:60–72.

2. Minnick MF, Raghavan R. 2012. Developmental biology of *Coxiella burnetii*. Adv Exp Med Biol 984:231–248.

3. van Schaik EJ, Chen C, Mertens K, Weber MM, Samuel JE. 2013. Molecular pathogenesis of the obligate intracellular bacterium *Coxiella burnetii*. Nat Rev Microbiol 11:561–573.

4. Dragan AL, Voth DE. 2020. *Coxiella burnetii*: international pathogen of mystery. Microbes Infect 22:100–110.

5. Larson CL, Martinez E, Beare PA, Jeffrey B, Heinzen RA, Bonazzi M. 2016. Right on Q: genetics begin to unravel *Coxiella burnetii* host cell interactions. Future Microbiol 11:919–939.

6. Newton P, Thomas DR, Reed SCO, Lau N, Xu B, Ong SY, Pasricha S, Madhamshettiwar PB, Edgington-Mitchell LE, Simpson KJ, Roy CR, Newton HJ. 2020. Lysosomal degradation products induce *Coxiella burnetii* virulence. Proc Natl Acad Sci USA 117:6801–6810.

7. Sireci G, Badami GD, Di Liberto D, Blanda V, Grippi F, Di Paola L, Guercio A, de la Fuente J, Torina A. 2021. Recent Advances on the Innate Immune Response to *Coxiella burnetii*. Front Cell Infect Microbiol 11:754455.

8. Lührmann A, Roy CR. 2007. *Coxiella burnetii* inhibits activation of host cell apoptosis through a mechanism that involves preventing cytochrome c release from mitochondria. Infect Immun 75:5282–5289.

9. Mulye M, Samanta D, Winfree S, Heinzen RA, Gilk SD. 2017. Elevated cholesterol in the *Coxiella burnetii* intracellular niche is bacteriolytic. MBio 8:e02313-16.

10. Siadous FA, Cantet F, Van Schaik E, Burette M, Allombert J, Lakhani A, Bonaventure B, Goujon C, Samuel J, Bonazzi M, Martinez E. 2021. *Coxiella* effector protein CvpF subverts RAB26-dependent autophagy to promote vacuole biogenesis and virulence. Autophagy 17:706–722.

11. Larson CL, Beare PA, Howe D, Heinzen RA. 2013. *Coxiella burnetii* effector protein subverts clathrin-mediated vesicular trafficking for pathogen vacuole biogenesis. Proc Natl Acad Sci USA 110:E4770-9.

12. Voth DE. 2016. Subversion of macrophage autophagy and inflammatory pathways by *Coxiella burnetii*. The Journal of Immunology 196:131.1-131.1.

358 13. Voth DE, Howe D, Heinzen RA. 2007. *Coxiella burnetii* inhibits apoptosis in human THP-1
359 cells and monkey primary alveolar macrophages. Infect Immun 75:4263–4271.

360 14. Macdonald LJ, Graham JG, Kurten RC, Voth DE. 2014. *Coxiella burnetii* exploits host
361 cAMP-dependent protein kinase signalling to promote macrophage survival. Cell Microbiol
362 16:146–159.

363 15. Vázquez CL, Colombo MI. 2010. *Coxiella burnetii* modulates Beclin 1 and Bcl-2, preventing
364 host cell apoptosis to generate a persistent bacterial infection. Cell Death Differ 17:421–438.

365 16. Klingenbeck L, Eckart RA, Berens C, Lührmann A. 2013. The *Coxiella burnetii* type IV
366 secretion system substrate CaeB inhibits intrinsic apoptosis at the mitochondrial level. Cell
367 Microbiol 15:675–687.

368 17. Winchell CG, Graham JG, Kurten RC, Voth DE. 2014. *Coxiella burnetii* type IV secretion-
369 dependent recruitment of macrophage autophagosomes. Infect Immun 82:2229–2238.

370 18. Gutierrez MG, Vázquez CL, Munafó DB, Zoppino FCM, Berón W, Rabinovitch M,
371 Colombo MI. 2005. Autophagy induction favours the generation and maturation of the *Coxiella*-
372 replicative vacuoles. Cell Microbiol 7:981–993.

373 19. Larson CL, Sandoz KM, Cockrell DC, Heinzen RA. 2019. Noncanonical inhibition of
374 mTORC1 by *Coxiella burnetii* promotes replication within a phagolysosome-like vacuole. mBio
375 10:e02816-18.

376 20. Bartel DP. 2018. Metazoan MicroRNAs. Cell 173:20–51.

377 21. Gebert LFR, MacRae IJ. 2019. Regulation of microRNA function in animals. Nat Rev Mol
378 Cell Biol 20:21–37.

379 22. Vasudevan S, Tong Y, Steitz JA. 2007. Switching from repression to activation: microRNAs

380 can up-regulate translation. Science 318:1931–1934.

381 23. Agarwal V, Bell GW, Nam J-W, Bartel DP. 2015. Predicting effective microRNA target sites
382 in mammalian mRNAs. eLife 4.

383 24. Wang W, Cai Y, Deng G, Yang Q, Tang P, Wu M, Yu Z, Yang F, Chen J, Werz O, Chen X.
384 2020. Allelic-specific regulation of xCT expression increases susceptibility to tuberculosis by
385 modulating microRNA-mRNA interactions. mSphere 5:e00263-20.

386 25. Huang T, Huang X, Yao M. 2018. miR-143 inhibits intracellular *Salmonella* growth by
387 targeting ATP6V1A in macrophage cells in pig. Res Vet Sci 117:138–143.

388 26. Janssen HLA, Reesink HW, Lawitz EJ, Zeuzem S, Rodriguez-Torres M, Patel K, van der
389 Meer AJ, Patick AK, Chen A, Zhou Y, Persson R, King BD, Kauppinen S, Levin AA, Hodges
390 MR. 2013. Treatment of HCV infection by targeting microRNA. N Engl J Med 368:1685–1694.

391 27. Koriyama T, Yamakuchi M, Takenouchi K, Oyama Y, Takenaka H, Nagakura T, Masamoto
392 I, Hashiguchi T. 2019. *Legionella pneumophila* infection-mediated regulation of RICTOR via
393 miR-218 in U937 macrophage cells. Biochem Biophys Res Commun 508:608–613.

394 28. Liu N, Wang L, Sun C, Yang L, Sun W, Peng Q. 2016. MicroRNA-125b-5p suppresses
395 *Brucella abortus* intracellular survival via control of A20 expression. BMC Microbiol 16:171.

396 29. Pierce JB, Simion V, Icli B, Pérez-Cremades D, Cheng HS, Feinberg MW. 2020.
397 Computational analysis of targeting SARS-CoV-2, viral entry proteins ACE2 and TMPRSS2,
398 and interferon genes by host microRNAs. Genes (Basel) 11:1354.

399 30. Schulte LN, Westermann AJ, Vogel J. 2013. Differential activation and functional
400 specialization of miR-146 and miR-155 in innate immune sensing. Nucleic Acids Res 41:542–
401 553.

402 31. Tamgue O, Gcanga L, Ozturk M, Whitehead L, Pillay S, Jacobs R, Roy S, Schmeier S,
403 Davids M, Medvedeva YA, Dheda K, Suzuki H, Brombacher F, Guler R. 2019. Differential
404 targeting of c-Maf, Bach-1, and Elmo-1 by microRNA-143 and microRNA-365 promotes the
405 intracellular growth of *Mycobacterium tuberculosis* in alternatively IL-4/IL-13 activated
406 macrophages. Front Immunol 10:421.

407 32. Bettencourt P, Marion S, Pires D, Santos LF, Lastrucci C, Carmo N, Blake J, Benes V,
408 Griffiths G, Neyrolles O, Lugo-Villarino G, Anes E. 2013. Actin-binding protein regulation by
409 microRNAs as a novel microbial strategy to modulate phagocytosis by host cells: the case of N-
410 Wasp and miR-142-3p. Front Cell Infect Microbiol 3:19.

411 33. Kim JK, Yuk J-M, Kim SY, Kim TS, Jin HS, Yang C-S, Jo E-K. 2015. MicroRNA-125a
412 inhibits autophagy activation and antimicrobial responses during Mycobacterial infection. J
413 Immunol 194:5355–5365.

414 34. Millar JA, Valdés R, Kacharia FR, Landfear SM, Cambronne ED, Raghavan R. 2015.
415 *Coxiella burnetii* and *Leishmania mexicana* residing within similar parasitophorous vacuoles
416 elicit disparate host responses. Front Microbiol 6:794.

417 35. Coleman SA, Fischer ER, Howe D, Mead DJ, Heinzen RA. 2004. Temporal analysis of
418 *Coxiella burnetii* morphological differentiation. J Bacteriol 186:7344–7352.

419 36. Krämer A, Green J, Pollard J, Tugendreich S. 2014. Causal analysis approaches in Ingenuity
420 Pathway Analysis. Bioinformatics 30:523–530.

421 37. Das K, Garnica O, Dhandayuthapani S. 2016. Modulation of host miRNAs by intracellular
422 bacterial pathogens. Front Cell Infect Microbiol 6:79.

423 38. Cordsmeier A, Wagner N, Lührmann A, Berens C. 2019. Defying death - how *Coxiella*

424 *burnetii* copes with intentional host cell suicide. Yale J Biol Med 92:619–628.

425 39. Voth DE, Heinzen RA. 2009. Sustained activation of Akt and Erk1/2 is required for *Coxiella*
426 *burnetii* antiapoptotic activity. Infect Immun 77:205–213.

427 40. Schäfer W, Eckart RA, Schmid B, Cagköylü H, Hof K, Muller YA, Amin B, Lührmann A.
428 2017. Nuclear trafficking of the anti-apoptotic *Coxiella burnetii* effector protein AnkG requires
429 binding to p32 and Importin-α1. Cell Microbiol 19.

430 41. Hatzimichael E, Dasoula A, Igglezou M, Katsenos A, Sainis I, Rigoutsos I, Briasoulis E.
431 2015. Expression profiling of a panel of apoptosis related microRNAs in patients with acute
432 myeloid leukemia. Blood 126:4971–4971.

433 42. He M, Wu N, Leong MC, Zhang W, Ye Z, Li R, Huang J, Zhang Z, Li L, Yao X, Zhou W,
434 Liu N, Yang Z, Dong X, Li Y, Chen L, Li Q, Wang X, Wen J, Zhao X, Hu R. 2020. miR-145
435 improves metabolic inflammatory disease through multiple pathways. J Mol Cell Biol 12:152–
436 162.

437 43. Mambu J, Barilleau E, Fragnet-Trapp L, Le Vern Y, Olivier M, Sadrin G, Grépinet O, Taieb
438 F, Velge P, Wiedemann A. 2020. Rck of *Salmonella* Typhimurium delays the host cell cycle to
439 facilitate bacterial invasion. Front Cell Infect Microbiol 10:586934.

440 44. Takai T, Tsujino T, Yoshikawa Y, Inamoto T, Sugito N, Kuranaga Y, Heishima K, Soga T,
441 Hayashi K, Miyata K, Kataoka K, Azuma H, Akao Y. 2019. Synthetic miR-143 exhibited an
442 anti-cancer effect via the downregulation of K-RAS networks of renal cell cancer cells in vitro
443 and in vivo. Mol Ther 27:1017–1027.

444 45. Liu L, Yu X, Guo X, Tian Z, Su M, Long Y, Huang C, Zhou F, Liu M, Wu X, Wang X.
445 2012. miR-143 is downregulated in cervical cancer and promotes apoptosis and inhibits tumor

formation by targeting Bcl-2. Mol Med Report 5:753–760.

46. Liu M, Jia J, Wang X, Liu Y, Wang C, Fan R. 2018. Long non-coding RNA HOTAIR promotes cervical cancer progression through regulating BCL2 via targeting miR-143-3p. Cancer Biol Ther 19:391–399.

47. Pugazhenthi S, Nesterova A, Sable C, Heidenreich KA, Boxer LM, Heasley LE, Reusch JE. 2000. Akt/protein kinase B up-regulates Bcl-2 expression through cAMP-response element-binding protein. J Biol Chem 275:10761–10766.

48. Krakauer T. 2019. Inflammasomes, Autophagy, and Cell Death: The Trinity of Innate Host Defense against Intracellular Bacteria. Mediators Inflamm 2019:2471215.

49. Latomanski EA, Newton HJ. 2018. Interaction between autophagic vesicles and the *Coxiella*-containing vacuole requires CLTC (clathrin heavy chain). Autophagy 14:1710–1725.

50. Martinez E, Allombert J, Cantet F, Lakhani A, Yandrapalli N, Neyret A, Norville IH, Favard C, Muriaux D, Bonazzi M. 2016. *Coxiella burnetii* effector CvpB modulates phosphoinositide metabolism for optimal vacuole development. Proc Natl Acad Sci USA 113:E3260-9.

51. Manning BD, Toker A. 2017. AKT/PKB signaling: navigating the network. Cell 169:381–405.

52. Hein AL, Ouellette MM, Yan Y. 2014. Radiation-induced signaling pathways that promote cancer cell survival. Int J Oncol 45:1813–1819.

53. Eckart RA, Bisle S, Schulze-Luehrmann J, Wittmann I, Jantsch J, Schmid B, Berens C, Lührmann A. 2014. Antiapoptotic activity of *Coxiella burnetii* effector protein AnkG is controlled by p32-dependent trafficking. Infect Immun 82:2763–2771.

54. Chung CY-S, Shin HR, Berdan CA, Ford B, Ward CC, Olzmann JA, Zoncu R, Nomura DK.

468 2019. Covalent targeting of the vacuolar H+-ATPase activates autophagy via mTORC1
469 inhibition. Nat Chem Biol 15:776–785.

470 55. Mukhopadhyay S, Biancur DE, Parker SJ, Yamamoto K, Banh RS, Paulo JA, Mancias JD,
471 Kimmelman AC. 2021. Autophagy is required for proper cysteine homeostasis in pancreatic
472 cancer through regulation of SLC7A11. Proc Natl Acad Sci USA 118.

473 56. Mauvezin C, Neufeld TP. 2015. Bafilomycin A1 disrupts autophagic flux by inhibiting both
474 V-ATPase-dependent acidification and Ca-P60A/SERCA-dependent autophagosome-lysosome
475 fusion. Autophagy 11:1437–1438.

476 57. Lin X-T, Zheng X-B, Fan D-J, Yao Q-Q, Hu J-C, Lian L, Wu X-J, Lan P, He X-S. 2018.
477 MicroRNA-143 targets ATG2B to inhibit autophagy and increase inflammatory responses in
478 Crohn's disease. Inflamm Bowel Dis 24:781–791.

479 58. Romano PS, Gutierrez MG, Berón W, Rabinovitch M, Colombo MI. 2007. The autophagic
480 pathway is actively modulated by phase II *Coxiella burnetii* to efficiently replicate in the host
481 cell. Cell Microbiol 9:891–909.

482 59. Dragan AL, Kurten RC, Voth DE. 2019. Characterization of early stages of human alveolar
483 infection by the Q fever agent *Coxiella burnetii.* Infect Immun 87:e00028-19.

484 60. Ke Y, Chen X, Su Y, Chen C, Lei S, Xia L, Wei D, Zhang H, Dong C, Liu X, Yin F. 2021.
485 Low expression of SLC7A11 confers drug resistance and worse survival in ovarian cancer via
486 inhibition of cell autophagy as a competing endogenous RNA. Front Oncol 11:744940.

487 61. Sandoz KM, Beare PA, Cockrell DC, Heinzen RA. 2016. Complementation of arginine
488 auxotrophy for genetic transformation of *Coxiella burnetii* by use of a defined axenic medium.
489 Appl Environ Microbiol 82:3042–3051.

490 62. Zhang W, Chen P, Zong H, Ding Y, Yan R. 2020. miR-143-3p targets ATG2B to inhibit
491 autophagy and promote endothelial progenitor cells tube formation in deep vein thrombosis.
492 Tissue Cell. 67:101453.

493 63. Omsland A, Cockrell DC, Howe D, Fischer ER, Virtaneva K, Sturdevant DE, Porcella SF,
494 Heinzen RA. 2009. Host cell-free growth of the Q fever bacterium *Coxiella burnetii*. Proc Natl
495 Acad Sci USA 106:4430–4434.

496 64. Martinez E, Cantet F, Bonazzi M. 2015. Generation and multi-phenotypic high-content
497 screening of *Coxiella burnetii* transposon mutants. J Vis Exp e52851.

498 65. Moses AS, Millar JA, Bonazzi M, Beare PA, Raghavan R. 2017. Horizontally acquired
499 biosynthesis genes boost *Coxiella burnetii*'s physiology. Front Cell Infect Microbiol 7:174.

500 66. Graham JG, Winchell CG, Kurten RC, Voth DE. 2016. Development of an ex vivo tissue
501 platform to study the human lung response to *Coxiella burnetii*. Infect Immun 84:1438–1445.

502 67. Ganesan S, Roy CR. 2019. Host cell depletion of tryptophan by IFNγ-induced Indoleamine
503 2,3-dioxygenase 1 (IDO1) inhibits lysosomal replication of *Coxiella burnetii*. PLoS Pathog
504 15:e1007955.

505 68. Sanchez SE, Vallejo-Esquerra E, Omsland A. 2018. Use of axenic culture tools to study
506 *Coxiella burnetii*. Curr Protoc Microbiol 50:e52.

507 69. Hayek I, Fischer F, Schulze-Luehrmann J, Dettmer K, Sobotta K, Schatz V, Kohl L, Boden
508 K, Lang R, Oefner PJ, Wirtz S, Jantsch J, Lührmann A. 2019. Limitation of TCA cycle
509 intermediates represents an oxygen-independent nutritional antibacterial Eefector mechanism of
510 macrophages. Cell Rep 26:3502-3510.e6.

511 70. Kozomara A, Birgaoanu M, Griffiths-Jones S. 2019. miRBase: from microRNA sequences to

512 function. Nucleic Acids Res 47:D155–D162.

513 71. Tweedie S, Braschi B, Gray K, Jones TEM, Seal RL, Yates B, Bruford EA. 2021.
514 Genenames.org: the HGNC and VGNC resources in 2021. Nucleic Acids Res 49:D939–D946.

515 72. Love MI, Huber W, Anders S. 2014. Moderated estimation of fold change and dispersion for
516 RNA-seq data with DESeq2. Genome Biol 15:550.

517 73. Livak KJ, Schmittgen TD. 2001. Analysis of relative gene expression data using real-time
518 quantitative PCR and the 2(-Delta Delta C(T)) Method. Methods 25:402–408.

519 74. Sachan M, Srivastava A, Ranjan R, Gupta A, Pandya S, Misra A. 2016. Opportunities and
520 challenges for host-directed therapies in tuberculosis. Curr Pharm Des 22:2599–2604.

521 75. Zhou J, Tan S-H, Nicolas V, Bauvy C, Yang N-D, Zhang J, Xue Y, Codogno P, Shen H-M.
522 2013. Activation of lysosomal function in the course of autophagy via mTORC1 suppression and
523 autophagosome-lysosome fusion. Cell Res 23:508–523.

524 76. Rontogianni S, Iskit S, van Doorn S, Peeper DS, Altelaar M. 2020. Combined EGFR and
525 ROCK inhibition in triple-negative breast cancer leads to cell death via impaired autophagic flux.
526 Mol Cell Proteomics 19:261–277.

527 77. Stankov M, Panayotova-Dimitrova D, Leverkus M, Klusmann J-H, Behrens G. 2014. Flow
528 cytometric analysis of autophagic activity with Cyto-ID staining in primary cells. Bio Protoc 4.

529 78. Plubell DL, Wilmarth PA, Zhao Y, Fenton AM, Minnier J, Reddy AP, Klimek J, Yang X,
530 David LL, Pamir N. 2017. Extended multiplexing of tandem mass tags (TMT) labeling reveals
531 age and high fat diet specific proteome changes in mouse epididymal adipose tissue. Mol Cell
532 Proteomics 16:873–890.

533

FIGURE LEGENDS

Figure 1. Host pathways potentially regulated by miRNAs during *C. burnetii* infection. Top 20 miRNA-targeted pathways significantly impacted in THP-1 macrophages infected with NMII. Orange bars show pathways that are putatively activated (z-score ≥ 1.5), and blue bars correspond to pathways that were predicted to be inhibited (z-score ≤1.5) using ingenuity pathway analysis (IPA). See full list in **Table S3**.

Figure 2. miR-143-3p expression is down-regulated in *C. burnetii*-infected macrophages. (**A**) Expression of miR-143-3p measured via RNA-seq (n = 3; 72 hpi) in NMII-infected THP-1 cells compared to uninfected cells. (**B**) Primary human alveolar macrophages (hAMs) infected with NMI or NMII or uninfected controls were analyzed for miR-143-3p expression using qRT-PCR at 72 hpi. Statistical significance in (A) was calculated using two-tailed paired Student's t-test followed by Welch's correction, and in (B) using one-way ANOVA followed by Tukey's multiple comparison test (n = 3).

Figure 3. Intracellular growth of *C. burnetii* is inhibited in the presence of excessive miR-143-3p. Quantification of intracellular *C. burnetii* at 48 hpi using qPCR (**A**) or CFU assay (**B**) in miR-143-3p-transfected HeLa cells compared to untransfected cells (Mock) and cells transfected with non-specific control miRNA (miR-control). Statistical significance was determined using one-way ANOVA followed by Tukey's multiple comparison test (ns: non-significant, n = 3).

Figure 4. miR-143-3p transfection promotes early apoptosis. Percentage of early (**A**) or late (**B**) apoptotic HeLa cells transfected with either miR-143-3p or a non-specific control miRNA

(miR-control). Early apoptosis (Annexin V-PE positive and eFluor780 negative) and late apoptosis/necrosis (Annexin V-PE positive and eFluor780 positive) were quantified by flow cytometry. Statistical significance was determined using two-tailed paired Student's t-test followed by Welch's correction (n = 3).

Figure 5. Increased miR-143-3p expression leads to reduced expression of apoptosis-related genes. (**A**) Expression (fold change) of *akt1* and *bcl2* genes in HeLa cells transfected with miR-143-3p compared to cells transfected with control miRNA (miR-control) measured using qRT-PCR. Statistical significance was determined using two-tailed paired t-test followed by Welch's correction (n = 3). (**B**) Fold change in phosphorylated Akt (pSer473) and Bcl-2 (pSer70) proteins in HeLa cells transfected with miR-143-3p compared to cells transfected with miR-control measured using a multiplex immunoassay. Activated proteins were measured as median fluorescence intensity and statistical significance was determined using two-tailed paired Student's t-test followed by Welch's correction (n = 3).

Figure 6. miR-143-3p inhibits autophagic flux. Y-axis shows relative autophagy flux reported as average brightness of CYTO-ID green (a cationic tracer that selectively labels autophagic compartments) per cell in miR-143-3p-transfected Hela cells compared to cells transfected with control miRNA (miR-control). Average CYTO-ID green brightness values were calculated from three sets of at least 200 cells per well and statistical significance was determined using two-tailed paired Student's t-test followed by Welch's correction (n = 3).

Figure 7. Transfection of HeLa cells with miR-143-3p decreased *atp6v1a*/VATA and *slc7a11*/xCT expression. (A) *atp6v1a* and *slc7a11* gene expression (fold change) in HeLa cells transfected with miR-143-3p compared to cells transfected with control miRNA (miR-control) measured using qRT-PCR. (**B**) VATA (encoded by *atp6v1a*) and xCT (encoded by *slc7a11*) proteins (fold change) in HeLa cells transfected with miR-143-3p compared to cells transfected with miR-control measured using quantitative mass-spectrometry. Statistical significance was determined using two-tailed paired Student's t-test followed by Welch's correction (n = 3).

589 **Table 1.** Number of differentially-expressed miRNAs and mRNAs in *C. burnetii*-infected THP-1
590 macrophages.

	miRNA[a]			**mRNA**[a]		
Time	**Total**[b]	**Down**	**Up**	**Total**[b]	**Down**	**Up**
8 hpi	25	12	13	454	220	234
24 hpi	25	16	9	1,160	665	495
48 hpi	35	23	12	1,742	445	1,297
72 hpi	60	43	17	6,525	3,236	3,289
120 hpi	34	18	16	211	80	131

591

592 [a]The current build of the human genome (GRCh38) has 2,654 mature miRNA sequences and
593 19,231 protein-coding genes.

594 [b]Differential expression ($\log_2$ fold change ≥ 0.75; Padj ≤ 0.05, Wald test) at respective hours
595 post-infection (hpi) was calculated using DESeq2 (72).

596

597

598

599

600

601 **Table 2.** Differentially-expressed ($p \leq 0.05$, $n = 3$) miRNAs in NMII-infected THP-1 cells

602 compared to uninfected controls.

603

miRNA	Fold Change	p-value
hsa-miR-708-5p	0.6225	0.037471
hsa-miR-145-5p	0.6312	0.006722
hsa-miR-143-3p	0.6535	0.007199
hsa-miR-106b-5p	0.7386	0.032799
hsa-miR-181d-5p	0.7611	0.028265
hsa-miR-16-5p	0.8026	0.024211
hsa-miR-222-3p	0.8804	0.014724
hsa-miR-365b-3p	1.1015	0.016939
hsa-miR-218-5p	1.5832	0.013546
hsa-miR-125a-5p	1.5868	0.010438
hsa-miR-192-5p	1.7689	0.03232
hsa-miR-146a-5p	5.9635	0.000006

604

605

606

SUPPLEMENTARY FIGURE

Figure S1. PI3K/Akt signaling network. Activation of PI3K by pro-survival stimuli leads to phosphorylation/activation of Akt. Akt in turn activates anti-apoptotic proteins and pro-survival transcription factor NF-κB, which leads to the induction of pro-survival proteins Bcl-2 and Bcl-xL, and activation of XIAP. Bcl-2 prevents the release of cytochrome c from mitochondria, thereby preventing apoptosis. Inhibition of *akt1* and *bcl2* expression by miR-143-3p (44–47), shown in red, could reverse this process to promote apoptosis.

SUPPLEMENTARY TABLES

Table S1. Differentially expressed miRNAs and mRNAs in NMII-infected THP-1 cells.

Table S2. Inverse expression pairs of differentially expressed miRNAs and target mRNAs.

Table S3. List of pathways enriched for miRNA-regulated genes.

Table S4. List of downregulated proteins in miR-143-3p-transfected HeLa cells identified using mass spectrometry.

Table S5. List of primers used in this study.

Figure 1

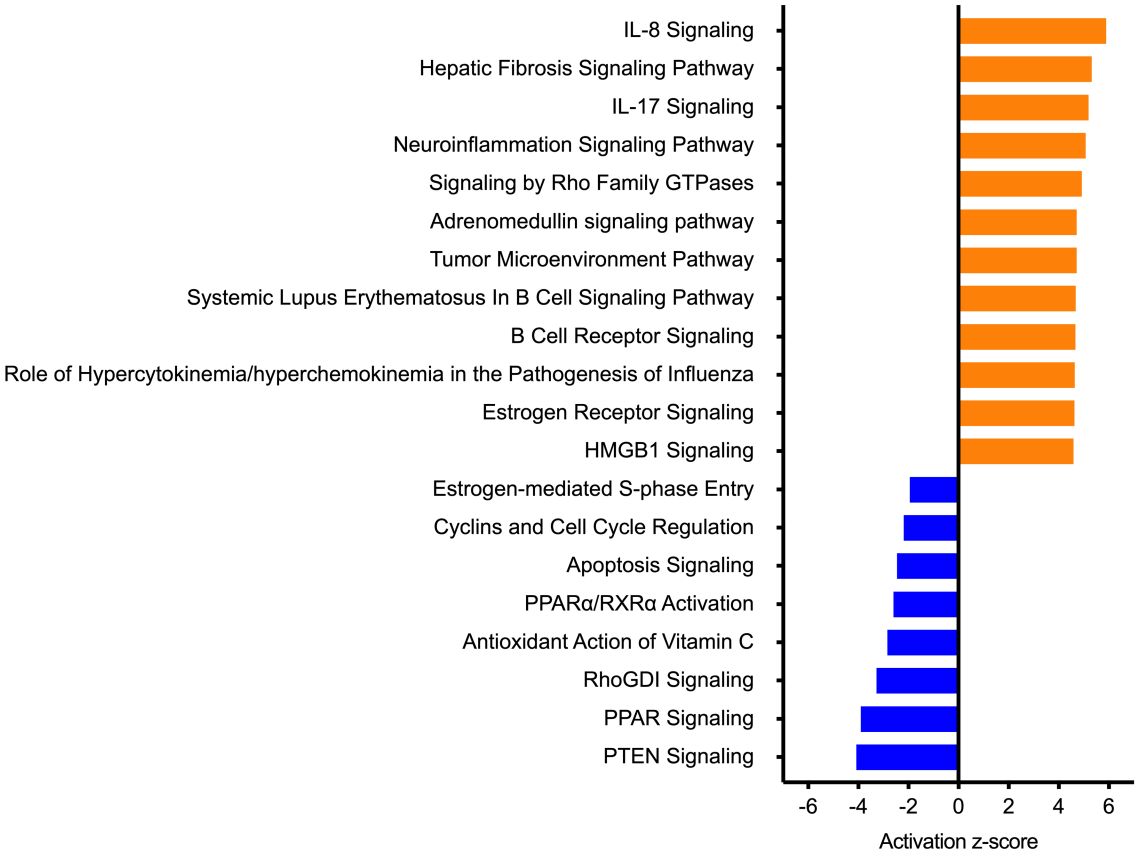

Figure 2

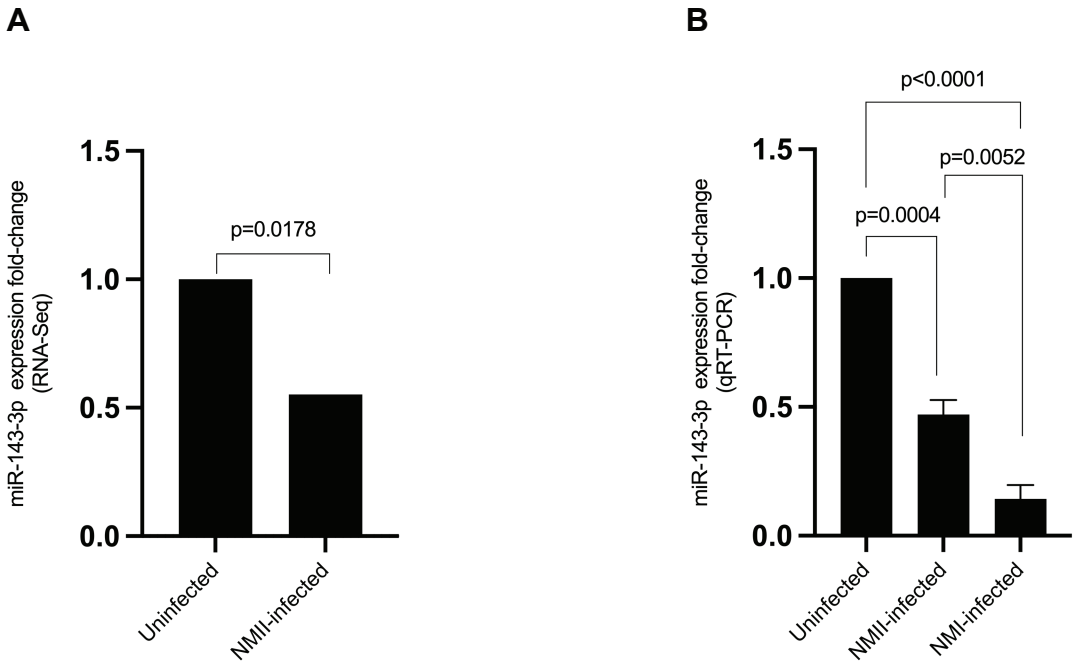

Figure 3

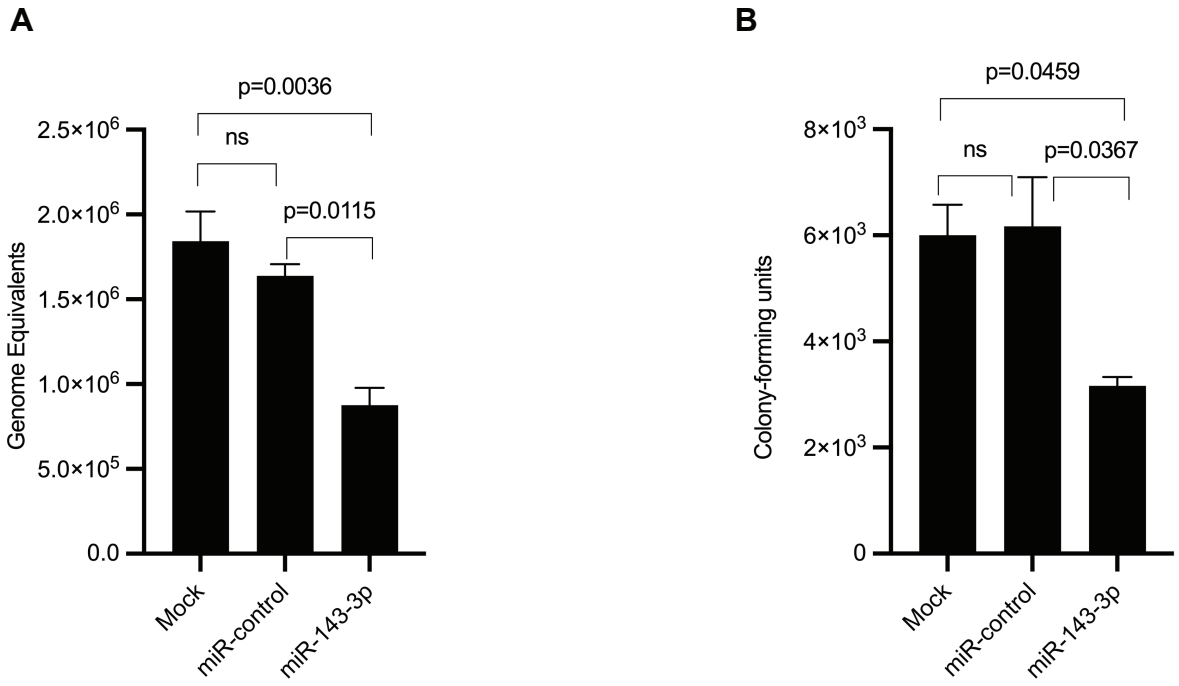

Figure 4

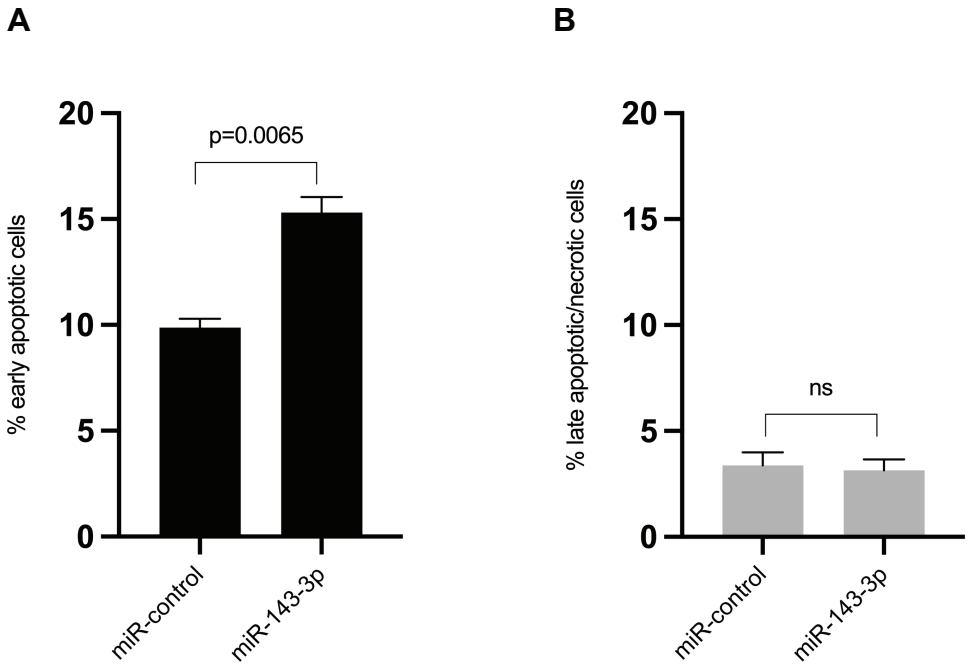

Figure 5

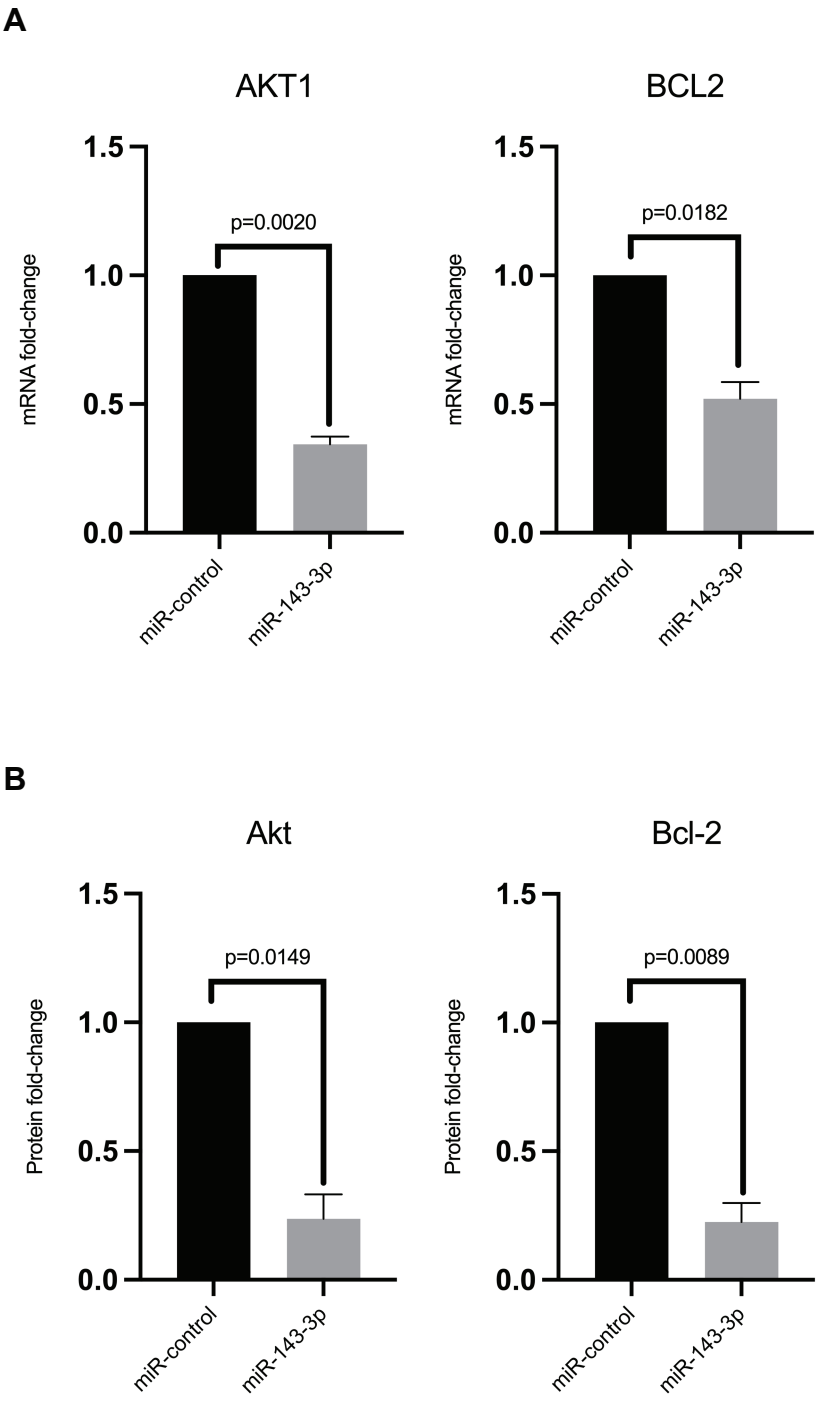

Figure 6

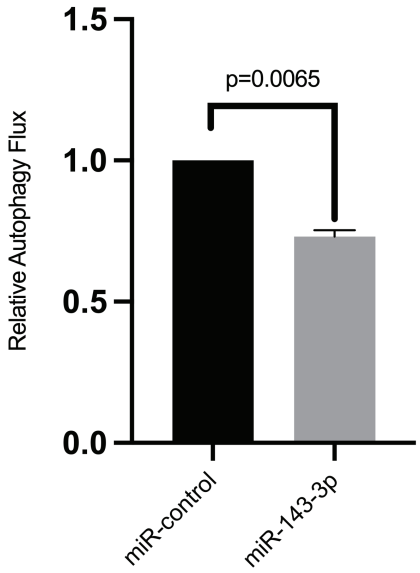

Figure 7